PROCEEDINGS OF SPIE

The high-contrast spectroscopy testbed for segmented telescopes (HCST): new wavefront control demonstrations

Jorge Llop-Sayson, Garreth Ruane, Nemanja Jovanovic, Dimitri Mawet, Daniel Echeverri, et al.

SPIE.

The high-contrast spectroscopy testbed for segmented telescopes (HCST): new wavefront control demonstrations

Jorge Llop-Sayson[a], Garreth Ruane[b,a], Nemanja Jovanovic[a], Dimitri Mawet[a,b], Daniel Echeverri[a], A J Eldorado Riggs[b], Carl T. Coker[b], Grady Morrissey[a], and He Sun[c]

[a]California Institute of Technology, 1200 E California Blvd., Pasadena, CA 91125
[b]Jet Propulsion Laboratory, California Institute of Technology, 4800 Oak Grove Drive, Pasadena, CA 91109
[c]Princeton University, Department of Mechanical & Aerospace Engineering, Equad Olden Street, Princeton, New Jersey 08544, United States

ABSTRACT

The High-Contrast Spectroscopy Testbed for Segmented Telescopes (HCST) in the Exoplanet Technology Laboratory (ET Lab) at Caltech is designed to test the technologies that will enable direct imaging and characterization of exoplanets with future segmented ground- and space-based telescopes. Wavefront sensing and control has been successfully implemented with electric field conjugation (EFC) using the FALCO Matlab package, yielding a baseline raw contrast of 1×10^{-8} in narrowband light with a Vector Vortex Coronagraph over a clear aperture. Here we report on progress towards our next HCST milestones: 1- Demonstration of 10^{-8} raw contrast levels in broadband light with the apodized vortex coronagraph using a LUVOIR B-like segmented aperture. 2- Integration of a fiber injection unit (FIU) and corresponding wavefront control algorithm to achieve 10^{-8} raw contrast in broadband light through a single mode fiber enabling high dispersion coronagraphy.

Keywords: High contrast imaging, Exoplanets, Wavefront Control, Wavefront Sensing, Spectroscopy

1. INTRODUCTION

Among the fascinating science cases the next generation of giant telescopes will undertake, both ground-based observatories, such as the Thirty Meter Telescope (TMT), and space-based telescopes, such as NASA's mission concept LUVOIR, direct imaging and characterization of atmospheres of nearby worlds remains one of the most compelling and challenging. Indeed, the contrast required for direct imaging of exoplanets, combined with the fact that large telescopes will likely be segmented, makes this task a colossal technology challenge. The High-Contrast Spectroscopy Testbed for Segmented Telescopes (HCST) is a high-contrast testbed aimed at developing technologies that will enable future imaging and characterization of exoplanets with segmented aperture telescopes. HCST is designed to replicate segmented telescope apertures, state-of-the-art coronagraph and adaptive optics (AO) systems, as well as science instruments, hence making it capable of addressing multiple technological challenges for space-based (LUVOIR, HabEx) and ground-based telescopes (TMT, E-ELT).

One of the main goals of HCST is to develop and test starlight suppression technologies for high-contrast imaging and spectroscopy of exoplanets, and thus improve the sensitivity of future instruments to fainter exoplanets. Demonstrating instrument concepts that will improve the final sensitivity to detecting molecules in exo-atmospheres is a high priority. We aim at demonstrating techniques such as high dispersion coronagraphy (HDC),[1–6] which combines high-contrast and high resolution spectroscopy to enhance detection of these evasive molecules.

High-contrast experiments have been running intensively at HCST for over a year with very encouraging results. Here we present the current status of HCST, and future plans for improvements and experiments. First, we report on the current layout of the testbed in Sec. 2, and the current wavefront sensing and control (WFSC)

Send correspondence to J. Llop-Sayson
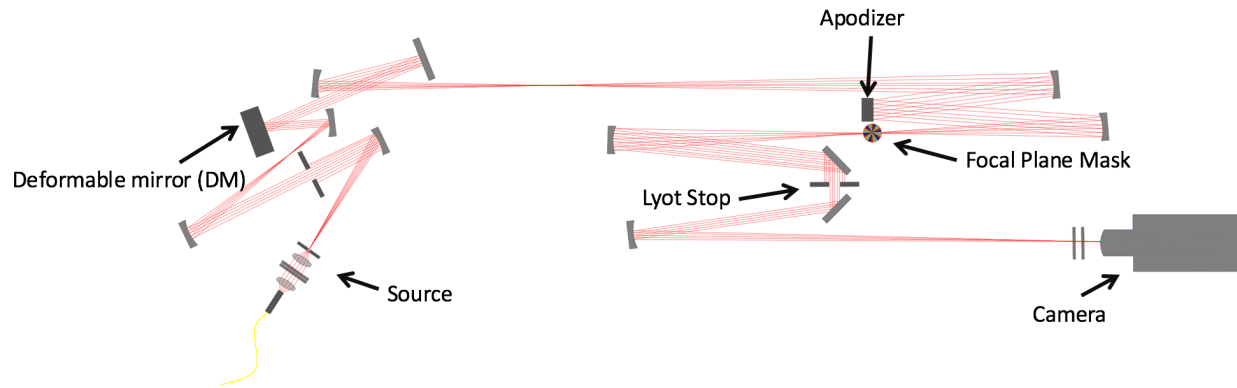E-mail: jllopsay@caltech.edu

Figure 1. HCST's current layout. At the position of the apodizer, when demonstrating the wavefront control capabilities of HCST, we placed a flat mirror to work with a circular clear aperture configuration, which is the one used for the results shown in Sec. 3. To test the apodized vortex coronagraph for segmented telescopes, we placed the prototype apodizer (see Sec. 4).

capabilities in Sec. 3. In Sec. 4, we give an update on the current experiments in which the first apodized vortex coronagraph[7] is being demonstrated at high-contrast. In Sec. 5 we present the plan for the next experiments at HCST that will consist on doing WFSC with single mode fibers (SMFs). Finally, in Sec. 6 we discuss the upgrades to improve the performance of HCST.

2. CURRENT LAYOUT

The current layout of HCST can be seen in Fig. 1. HCST's light source is a supercontinuum white light source (NKT Photonics SuperK EXTREME) that connects to a tunable filter (NKT Photonics SuperK VARIA), with which the wavelength and bandwidth of the light can be selected. The light is fed into the testbed with a single mode fiber (SMF), and then focused on a 5 μm pinhole. The AO system is equipped with a deformable mirror (DM), a Boston Micromachines kilo-DM, with 34×34 actuators. Following the beam, a flat mirror replaces the second DM, which will be included in the AO system in the future. The coronagraph system is a three-plane coronagraph with an apodizer plane, a focal plane mask (FPM), and a Lyot stop. The apodizer plane can either contain an apodizer or a flat mirror to simulate open circular apertures. At the focal plane, a vector vortex coronagraph mask is aligned to the pseudo-star to null its light. Vortex coronagraphs enable high throughput and high-contrast at small angular separations.[8,9] The Lyot stop blocks ∼93% of the radius of a 16.4 mm beam. The camera is an sCMOS (Andor Neo 5.5).

The testbed is isolated from the environment with a custom-made enclosure consisting of aluminum honeycomb panels designed to create a thermally stable environment, free from air turbulence, as well as with an optical table that provides vibration isolation through active damping. The PSF jitter is within ∼2% of λ/D, but there are some small PSF drifts, caused by small changes in gradients of temperature in the bench, with various orders of movement (from 0.1 to $1\lambda/D$) and different timescales (from a few hours to several days).

3. WAVEFRONT SENSING AND CONTROL CAPABILITIES

3.1 EFC with the FALCO Package

The algorithm used to perform wavefront sensing and control (WFSC) experiments and demonstrate high-contrast is the electric field conjugation (EFC) technique. EFC[10] finds the DM shape that minimizes the electric field at the image plane iteratively. EFC is a model-based algorithm; to obtain an estimate of the electric field, and to solve for optimal DM shape with the Jacobian of the system, an accurate optical model of the testbed is needed. The Jacobian contains the effect of each DM actuator on the electric field at the image plane. This technique has been demonstrated extensively on different testbeds,[11] and it is baselined to be the wavefront control algorithm used for the WFIRST-CGI.[12]
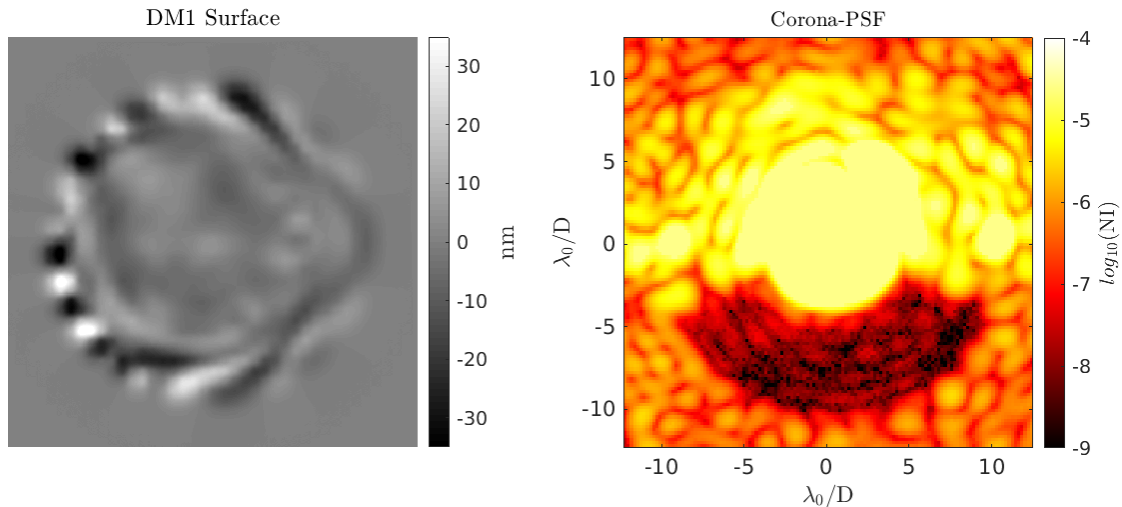
Figure 2. Result of a typical narrowband EFC run at HCST: solution for the DM shape (*left*), and coronagraphic PSF with the resulting dark hole (*right*). Levels of raw contrast of 10^{-8} are consistently reached at HCST.

All EFC experiments are run using the Matlab Fast Linear Least-Squares Coronagraph Optimization (FALCO) software package[13*], an open source toolbox to run testbeds, perform simulations, or do coronagraph design. FALCO provides a modular architecture, with the wavefront sensing modules included to perform the estimation of the electric field. One of the main advantages to using FALCO is the rapid computation of the Jacobian.

3.2 Narrowband Clear Aperture Experiments

The first EFC demonstration was with an open clear circular aperture configuration, i.e. without a segmented aperture or an apodizer. First, we tested for narrowband light, ~1% bandwidth at 775 nm. Before performing wavefront control, since EFC is greatly influenced by the accuracy of the optical model of the testbed, extensive work had to be done in this regard prior to reaching HCST's best WFSC capabilities. DM registration and characterization is crucial for a good EFC performance. Using our Zernike Wavefront Sensor (ZWFS),[14, 15] we are able to get an accurate registration of the DM actuators, i.e. their relative position with respect to the beam. Pupil imaging gives us the ability to determine the amplitude errors at the pupil plane. Next, a good understanding of polarization in the system was also crucial to reduce incoherent light. We were able to deal with polarization aberrations and leakage after a thorough inspection of several optics, and with a reconfiguration of the input light source. Furthermore, image sharpening via Zernike tuning with the DM, and with a full-control-area EFC, set the wavefront to an almost-flat starting point, ¡0.01 waves RMS.

Narrowband experiments yield an average raw contrast in the dark hole, i.e. the area in the image plane in which the electric field is nulled, of 10^{-8} levels. For a 60° arc dark hole, from 6 λ/D to 10 λ/D, the resulting average raw contrast is 1×10^{-8}. The DM shape we obtained, and its corresponding dark hole, are shown in Fig. 2. Because we only have one DM, we can only dig one-sided dark holes with the current configuration at HCST.

3.3 Broadband Clear Aperture Experiments

Broadband EFC relies on the same principle as regular monochromatic EFC, with the main difference being that the minimization is performed for the DM shape that minimizes several wavelengths at the same time. FALCO allows for easily running broadband EFC. Our broadband experiments are at 10% bandwidth at 775 nm, in which the control is made to work with 3 wavelengths over the bandpass. The NKT VARIA is controlled to select between different wavelengths during the EFC run.
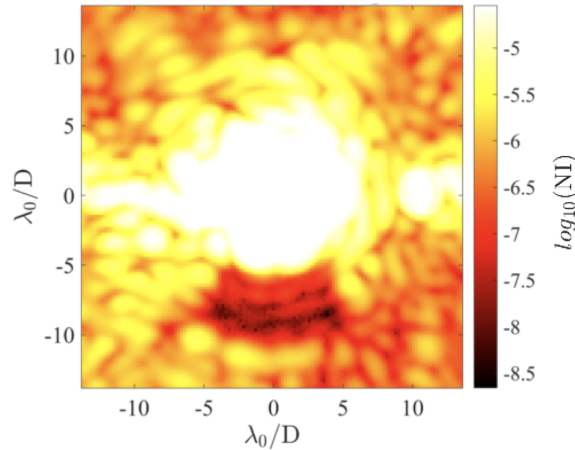
---

*https://github.com/ajeldorado/falco-matlab

Figure 3. Broadband coronagraphic PSF after wavefront correction over a $60°$ arc dark hole, from 6 λ/D to 10 λ/D. This is HCST's best broadband result with 3×10^{-8} raw contrast in a 10% bandpass.

Broadband WFSC presents its own challenges. Accounting for chromatic errors in the system is harder, as the mismatch between the model used for EFC and the real physical testbed is harder to overcome. However, given the quality of the optics, Lyot stop, and the extensive characterization we carried out for the narrowband demonstration, the expected results were obtained without much further work. Again, average raw contrast reaches levels of 10^{-8}, however, current limitations on the testbed hinder our WFSC capabilities for broadband light, making it harder with respect to narrowband WFSC. The $60°$ arc dark hole, with radius from 6 λ/D to 10 λ/D, yields a raw contrast of 3×10^{-8}. Fig. 3 shows a broadband coronagraphic PSF from one of the EFC runs.

The factor of ~ 3 difference between the achieved raw contrast with narrowband light and broadband light is probably due to chromatic errors within the system that are not well accounted in the Jacobian of the system when performing wavefront control with EFC.

3.4 System Identification at HCST

System Identification, or System ID, is an algorithm aimed at building mathematical models of physical systems, which was first applied to WFSC for high contrast imaging by Sun et al. (2019).[16] In this approach, System ID aims at improving the Jacobian of the system to account for model errors. The performance of EFC relies heavily on the accuracy of the optical model of the system; a model is needed for performing both the estimation of the electric field and the control of the wavefront. Via alignment and calibration, the numerical model can be improved. However, given the complexity of the system, these procedures have intrinsic uncertainties, which makes the resulting Jacobian imperfect.

A system ID algorithm helps with model uncertainty by using a neural network that iteratively optimizes the Jacobian. The model parameters are estimated as hidden variables within the neural network, and accounted in the resulting Jacobian to minimize the chosen cost function, e.g. the raw contrast. We use the Variational Learning (VL) algorithm with the TensorFlow Python package[†] to perform the optimization, and FALCO to perform the WFSC. The flowchart of the algorithm used in the System ID implementation at HCST can be seen in Fig. 4. EFC is run for a few iterations, in which all data is saved, i.e. all images and DM commands for both sensing and control steps, then, after EFC has run, this data is sent to the VL optimization, where the neural network, provided with a model of the physical processes based on Fourier optics, computes an improved Jacobian.

System ID was successfully implemented at HCST, providing gains in terms of final raw contrast of a factor of ~ 3, after 10 iterations of EFC. Another approach is to make System ID find an optimized DM actuator relative gain map, instead of trying to find the full Jacobian. The DM actuator relative gain map accounts for the effect
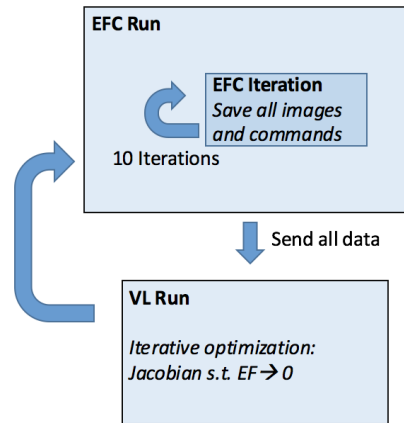

[†]https://www.tensorflow.org/

Figure 4. Flowchart of HCSTs implementation of System ID. With this SystemID approach using the Tensorflow package we achieve our best wavefront control performance, i.e. 1×10^{-8}, in less iterations.

that each DM actuator has on the image plane relative to one another, this variable has an important impact on the Jacobian. This approach was successful in providing a new gain map, which has a similar appearance to the map obtained with the ZWFS. Although this approach did not help with a better final raw contrast after a full run of EFC, a faster convergence was achieved, and thus the WFSC performance was improved. A faster control directly implies more time for science target exposure.

4. THE APODIZED VORTEX CORONAGRAPH EXPERIMENTS

In this section we discuss the preliminary results of the apodized vortex coronagraph (AVC) concept demonstration.

4.1 AVC concept

The levels of contrast required to directly image and characterize faint exoplanets is a tremendous task, especially when aiming at rocky companions orbiting Sun-like stars. For instance, the contrast required to image an Earth-like exoplanet around a Sun-like star is approximately of 1×10^{-10}. To make things worse, telescopes big enough to tackle this science case will most likely be segmented, which makes reaching high-contrast even more difficult. Indeed, discontinuities of any kind in the pupil, e.g. segmentation, an on-axis secondary mirror, or support structures, are very detrimental in terms of unwanted diffraction; the DM can hardly correct these kinds of errors without throwing away the sensitivity to circumstellar objects.

However, over the last decade, an array of clever solutions has been proposed to deal with these kinds of discontinuities.[7,17–27] For instance, the AVC handles the diffraction by apodizing the pupil plane upstream of a vortex coronagraph to create an area around the star free from diffraction artifacts resulting from segmentation.[7] The design of the apodizer is based on a gray-scaled apodization pattern numerically optimized to yield enhanced sensitivity to close-in circumstellar objects.

Simulations comparing the AVC concept to an unapodized segmented pupil in the style of LUVOIR-B show a significant improvement in terms of raw contrast achieved. In Fig. 5 we show two simulations of an HCST experiment using an unapodized segmented aperture versus the AVC design for the same aperture. The gains in terms of raw contrast are clear from the beginning; before running wavefront control, the apodizer is able to cancel the diffraction spikes that appear due to the hexagonal segmentation of a LUVOIR-B type aperture. This eases control by the DM, resulting in an improved final raw contrast.
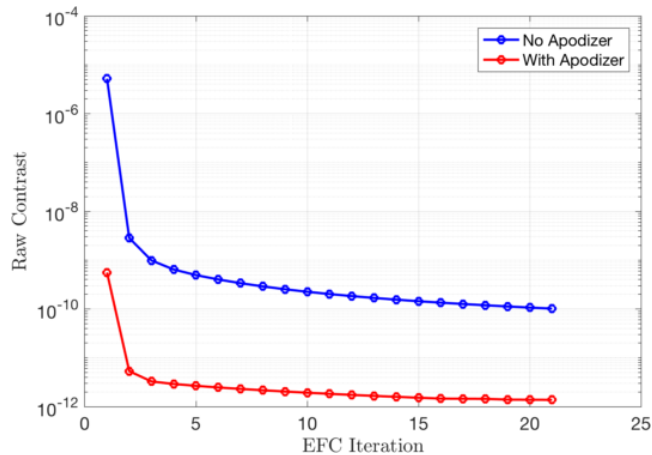
Figure 5. Simulations of the HCST setup for a LUVOIR-B type aperture for an unapodized pupil (blue), and an AVC for the same aperture (red). The simulation is for a one DM setup, the dark hole is one-sided, from 3 λ/D to 10 λ/D.
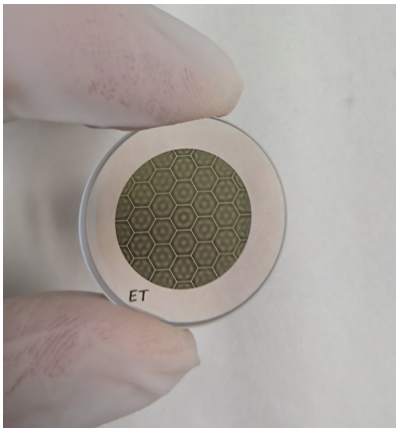

Figure 6. Picture of an apodizer prototype, based on the design for a LUVOIR-B type pupil. The experiments at HCST are done with this design. The microdot technique allows for a precise gray-scale pattern that grants the improved performance of the AVC with respect to a segmented unapodized aperture.

4.2 Laboratory results at HCST

A prototype was fabricated by Opto-Line to be tested at HCST and thus demonstrate the AVC concept for high-contrast imaging. Fig. 6 shows a prototype of the apodizer for these experiments. The gray-scale effect is achieved with the microdot technique, in which reflective gold microdots are evaporated onto the surface of the substrate. The approximate size of these microdots is ∼10 μm. The substrate is transmissive, made of AR-coated fused silica.

The result for a typical EFC run with the AVC at HCST with monochromatic light at 780 nm is shown in Fig. 7: on the left, the average raw contrast on the dark hole versus wavefront control iteration, and on the right, the resulting dark hole. Preliminary results of running EFC with the AVC consistently yield raw contrast levels of 10^{-8}. A raw contrast of $\sim 2 \times 10^{-8}$ is achieved for a 60° arc dark hole, with radius from 6 λ/D to 10 λ/D.

5. FIBER INJECTION UNIT EXPERIMENTS

Following the AVC laboratory demonstrations, our plan for future experiments involves a fiber injection unit (FIU) for experiments with single mode fibers (SMFs). The motivation for using single mode fibers in high-contrast imaging and spectroscopy of exoplanets comes from the modal selectivity of a SMF. Indeed, a planet
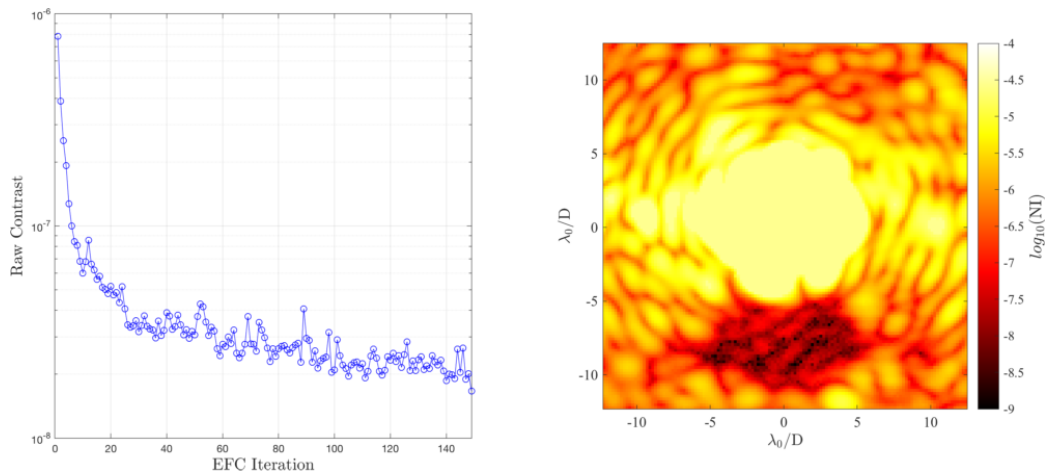
Figure 7. Apodized vortex coronagraph (AVC) testbed results of raw contrast for each EFC iteration (*left*), and the final coronagraphic PSF (*right*), for monochromatic light at 780 nm. The wavefront control tests for the AVC consistently reach levels close to 10^{-8} raw contrast.
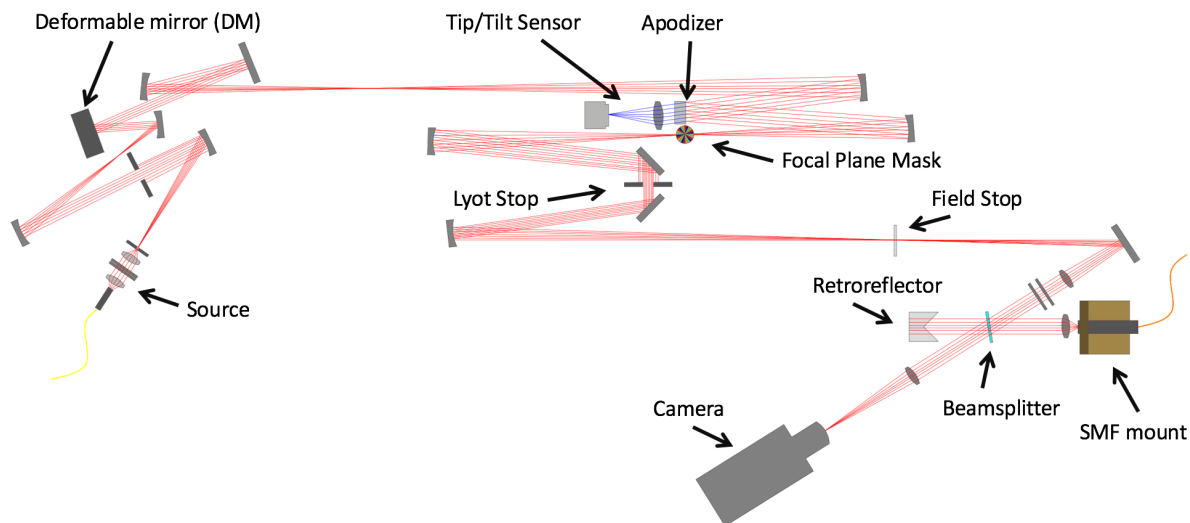

Figure 8. HCST's layout after current plans to add a fiber injection unit (FIU) for wavefront control experiments with single mode fibers, and introducing upgrades to improve the performance of the testbed. With the FIU we plan to do wavefront sensing and control through a single mode fiber[6, 28] to reach high levels of contrast, better that 10^{-8}, for broadband light.[29]

aligned with the SMF in the image plane will couple better than the stellar speckles, which allows for immediate improvement of unwanted stellar light rejection. The planet light is then sent to a spectrograph, with the hope of detecting molecular species of the exo-atmosphere, as conceived by the HDC concept.[5] We previously demonstrated in the laboratory wavefront control over a SMF to minimize the coupling of speckles through the fiber, with a technique based on speckle nulling,[6] and recently with a modified version of EFC.[28]

The layout of the FIU at HCST can be seen in Fig. 8. After the field stop (see Sec. 6) the light is collimated, circularly analyzed, and, with a beamsplitter plate, sent into the SMF. A lens to match the F/# of the SMF focuses the light onto the tip of the fiber. The HCST camera is used as a tracking camera. To calibrate the position of the fiber with the tracking camera, a corner cube acts as a retroreflector, so that the FIU can back-feed light into the system, which is focused into the camera indicating the position of the SMF.

The first experiment planned with the FIU is to perform WFSC with a SMF, and achieve high levels of

contrast for broad bandwidths through the fiber. We demonstrated a modified version of EFC that controls the coupled speckles that go through a fiber to achieve improved speckle suppression with respect to conventional EFC.[28] This modified version of EFC works with a similar mathematical formalism that, instead of working with the electric field at the pixels in the image plane, accounts for the coupling of the fiber, i.e. the overlap integral of the electric field with the fundamental mode of the fiber. Hence, in this case we work with one element, or *fibxel*, instead of with several conventional pixels. Previous experiments were performed at the transmissive version of HCST, with a lower order DM, and overall lower quality optics. We thus plan to demonstrate this technique for higher levels of contrast, and broader bandwidth. Simulations show that we will break the 10^{-8} raw contrast barrier through the SMF; we expect to reach levels of *SMF raw contrast*[28] of 10^{-9} with 10% broadband light at 775 nm. For these experiments we will use FALCO, as it already includes the modified version of EFC for SMFs.

Following the single SMF experiments, we plan to demonstrate the multi-object WFSC via SMFs (see Coker et al., these proceedings). This concept consists on placing several SMFs over an arbitrary number of circumstellar objects to feed their light into a spectrograph after performing WFSC simultaneously over the SMFs.[29] The prototype multi-SMFs fiber bundle has already been delivered to the laboratory, manufactured by Chiral Photonics. The WFSC algorithm, a modified version of EFC that performs control over more than one fibxel, is included in FALCO, and has been tested in simulation.

6. UPGRADES TO HCST

In this section we present the upgrades being worked on to improve the performance of HCST:

Source Reconfiguration: The source mount is the most probable cause of the PSF drifts in the testbed, so we plan on rebuilding it to make it more stable. The new source architecture will be more robust, without a 3-axis mount, and without the current standing rail structure in which the input fiber, the circular polarizer, and the pinhole are mounted. We plan on adding actuated rotation stages for the circular analyzer, and circular polarizer, to get better control of the polarization state through the testbed.

Field Stop: A field stop will be added at the image plane where the camera sits at the moment (see Fig. 8). With this change in the setup we aim to avoid ghosts in the system. The field stop blocks the bright parts of the field only letting through the area of interest that contains the dark hole. The camera we use has a glass window to allow cooling, which is prone to sending light back into the system, as well as inducing internal reflections within the camera. Furthermore, we want to be able to move the circular analyzer, consisting of two transmissive optics, downstream of the field stop.

Low Order Aberration Sensing and Control: Given that the apodizer substrate is transmissive, we plan on having a lens focus the collimated light that passes through the apodizer and focus is onto a small pixel camera to track the movement of the PSF (see Fig. 8). We will tip/tilt control the beam with a fast steering piezo actuator manufactured by Physics Instrument (PI), already available in the laboratory.

Environmental Sensing: A system of eight independent environmental sensors will be placed across the bench to track temperature, humidity, and 3-axis acceleration. A map of these variables throughout a wavefront control run will inform us on how the environment affects our performance. Furthermore, logging the state of the air in this way gives a start on learning how to incorporate environmental data into predictive control algorithms in the future.

7. CONCLUSION

Wavefront control at HCST has successfully demonstrated very high levels of contrast. The first demonstrations with a circular unobstructed aperture configuration consistently yield a raw contrast of 1×10^{-8} for narrowband light at 775 nm for a 60° arc dark hole, from 6 λ/D to 10 λ/D, and 3×10^{-8} for 10% broadband light at 775 nm for the same dark hole. We have demonstrated the apodized vortex coronagraph concept that corrects for segmentation in the pupil to high levels of contrast ($\sim2\times10^{-8}$ in laser light at 780 nm). This demonstration paves the way for a new family of coronagraphs that yield better sensitivity to exoplanets in the case of segmented telescope apertures, like the cases of future large telescopes TMT and LUVOIR. We are currently working on improving the performance of HCST. Limitations to the performance include a combination of model uncertainty,

PSF jitter and drift, ghosts from back reflections in the system and incoherent light, polarization aberration issues and leakage, and the least significant bit of the DM electronics. Plans to address these challenges include further work on the system ID algorithm to tackle the model mismatch problem, including a low order wavefront sensor, adding actuated rotation stages to the circular polarizer and circular analyzer, and adding a field stop to mitigate ghosts.

ACKNOWLEDGMENTS

REFERENCES

[1] Sparks, W. B. and Ford, H. C., "Imaging Spectroscopy for Extrasolar Planet Detection," **578**, 543–564 (Oct. 2002).

[2] Kawahara, H., Murakami, N., Matsuo, T., and Kotani, T., "Spectroscopic coronagraphy for planetary radial velocimetry of exoplanets," *The Astrophysical Journal Supplement Series* **212**, 27 (jun 2014).

[3] de Kok, R. J., Birkby, J., Brogi, M., Schwarz, H., Albrecht, S., de Mooij, E. J. W., and Snellen, I. A. G., "Identifying new opportunities for exoplanet characterisation at high spectral resolution," **561**, A150 (Jan. 2014).

[4] Snellen, I., de Kok, R., Birkby, J. L., Brandl, B., Brogi, M., Keller, C., Kenworthy, M., Schwarz, H., and Stuik, R., "Combining high-dispersion spectroscopy with high contrast imaging: Probing rocky planets around our nearest neighbors," **576**, A59 (Apr. 2015).

[5] Wang, J., Mawet, D., Ruane, G., Hu, R., and Benneke, B., "Observing Exoplanets with High Dispersion Coronagraphy. I. The Scientific Potential of Current and Next-generation Large Ground and Space Telescopes," *Astron. J.* **153**, 183 (Apr. 2017).

[6] Mawet, D., Ruane, G., Xuan, W., Echeverri, D., Klimovich, N., Randolph, M., Fucik, J., Wallace, J. K., Wang, J., Vasisht, G., Dekany, R., Mennesson, B., Choquet, E., Delorme, J.-R., and Serabyn, E., "Observing Exoplanets with High-dispersion Coronagraphy. II. Demonstration of an Active Single-mode Fiber Injection Unit," *Astrophys. J.* **838**, 92 (2017).

[7] Ruane, G., Jewell, J., Mawet, D., Pueyo, L., and Shaklan, S., "Apodized vortex coronagraph designs for segmented aperture telescopes," in [], *Society of Photo-Optical Instrumentation Engineers (SPIE) Conference Series* **9912**, 99122L (Jul 2016).

[8] Foo, G., Palacios, D. M., and Swartzlander, G. A., "Optical vortex coronagraph," *Opt. Lett.* **30**, 3308–3310 (2005).

[9] Mawet, D., Riaud, P., Absil, O., and Surdej, J., "Annular Groove Phase Mask Coronagraph," *Astrophys. J.* **633**, 1191–1200 (2005).

[10] Give'On, A., "A unified formailism for high contrast imaging correction algorithms," *Proc. SPIE* **7440**, 74400D (2009).

[11] Groff, T. D., Riggs, A., Kern, B., and Kasdin, N. J., "Methods and limitations of focal plane sensing, estimation, and control in high-contrast imaging," *J. Astron. Telesc. Instrum. Syst.* **2**(1), 011009 (2016).

[12] Spergel, D., Gehrels, N., Baltay, C., Bennett, D., Breckinridge, J., Donahue, M., Dressler, A., Gaudi, B. S., Greene, T., Guyon, O., Hirata, C., Kalirai, J., Kasdin, N. J., Macintosh, B., Moos, W., Perlmutter, S., Postman, M., Rauscher, B., Rhodes, J., Wang, Y., Weinberg, D., Benford, D., Hudson, M., Jeong, W.-S., Mellier, Y., Traub, W., Yamada, T., Capak, P., Colbert, J., Masters, D., Penny, M., Savransky, D., Stern, D., Zimmerman, N., Barry, R., Bartusek, L., Carpenter, K., Cheng, E., Content, D., Dekens, F., Demers, R., Grady, K., Jackson, C., Kuan, G., Kruk, J., Melton, M., Nemati, B., Parvin, B., Poberezhskiy, I., Peddie, C., Ruffa, J., Wallace, J. K., Whipple, A., Wollack, E., and Zhao, F., "Wide-Field InfrarRed Survey Telescope-Astrophysics Focused Telescope Assets WFIRST-AFTA 2015 Report," *ArXiv e-prints* , 1503.03757 (2015).

[13] Riggs, A. J. E., Ruane, G., Sidick, E., Coker, C., Kern, B. D., and Shaklan, S. B., "Fast linearized coronagraph optimizer (FALCO) I: a software toolbox for rapid coronagraphic design and wavefront correction," in [*Space Telescopes and Instrumentation 2018: Optical, Infrared, and Millimeter Wave*], *Society of Photo-Optical Instrumentation Engineers (SPIE) Conference Series* **10698**, 106982V (Aug. 2018).

[14] Wallace, J. K., Crawford, S., Loya, F., and Moore, J., "A phase-shifting zernike wavefront sensor for the palomar p3k adaptive optics system," (2012).

[15] N'Diaye, M., Vigan, A., Dohlen, K., Sauvage, J.-F., Caillat, A., Costille, A., Girard, J. H. V., Beuzit, J.-L., Fusco, T., Blanchard, P., Le Merrer, J., Le Mignant, D., Madec, F., Moreaux, G. Mouillet, D., Puget, P., and Zins, G., "Zelda, a zernike wavefront sensor for the fine measurement of quasi-static aberrations in coronographic systems: concept studies and results with vlt/sphere," (2016).

[16] Sun, H., Kasdin, N. J., and Vanderbei, R., "Identification and adaptive control of a high-contrast focal plane wavefront correction system," *Journal of Astronomical Telescopes, Instruments, and Systems* **4**(4), 1 – 15 – 15 (2018).

[17] Mawet, D., Serabyn, E., Wallace, J. K., and Pueyo, L., "Improved high-contrast imaging with on-axis telescopes using a multistage vortex coronagraph," *Optics Letters* **36**, 1506 (Apr 2011).

[18] Pueyo, L. and Norman, C., "High-contrast Imaging with an Arbitrary Aperture: Active Compensation of Aperture Discontinuities," **769**, 102 (Jun 2013).

[19] Mawet, D., Pueyo, L., Carlotti, A., Mennesson, B., Serabyn, E., and Wallace, J. K., "Ring-apodized Vortex Coronagraphs for Obscured Telescopes. I. Transmissive Ring Apodizers," **209**, 7 (Nov 2013).

[20] Carlotti, A., Pueyo, L., and Mawet, D., "Apodized phase mask coronagraphs for arbitrary apertures. II. Comprehensive review of solutions for the vortex coronagraph," **566**, A31 (Jun 2014).

[21] Guyon, O., Hinz, P. M., Cady, E., Belikov, R., and Martinache, F., "High Performance Lyot and PIAA Coronagraphy for Arbitrarily Shaped Telescope Apertures," **780**, 171 (Jan 2014).

[22] Ruane, G. J., Absil, O., Huby, E., Mawet, D., Delacroix, C., Carlomagno, B., Piron, P., and Swartzlander, G. A., "Optimized focal and pupil plane masks for vortex coronagraphs on telescopes with obstructed apertures," in [], *Society of Photo-Optical Instrumentation Engineers (SPIE) Conference Series* **9605**, 96051I (Sep 2015).

[23] Ruane, G. J., Huby, E., Absil, O., Mawet, D., Delacroix, C., Carlomagno, B., and Swartzlander, G. A., "Lyot-plane phase masks for improved high-contrast imaging with a vortex coronagraph," **583**, A81 (Nov 2015).

[24] Mazoyer, J., Pueyo, L., Norman, C., N'Diaye, M., Mawet, D., Soummer, R., Perrin, M., Choquet, É., and Carlotti, A., "Active correction of aperture discontinuities (ACAD) for space telescope pupils: a parametic analysis," in [], *Society of Photo-Optical Instrumentation Engineers (SPIE) Conference Series* **9605**, 96050M (Sep 2015).

[25] Balasubramanian, K., White, V., Yee, K., Echternach, P., Muller, R., Dickie, M., Cady, E., Prada, C. M., Ryan, D., Poberezhskiy, I., Kern, B., Zhou, H., Krist, J., Nemati, B., Eldorado Riggs, A. J., Zimmerman, N. T., and Kasdin, N. J., "WFIRST-AFTA coronagraph shaped pupil masks: design, fabrication, and characterization," *Journal of Astronomical Telescopes, Instruments, and Systems* **2**, 011005 (Jan 2016).

[26] Trauger, J. T., Moody, D. C., Krist, J. E., and Gordon, B. L., "Hybrid lyot coronagraph for wfirst-afta: coronagraph design and performance metrics," *Journal of Astronomical Telescopes, Instruments, and Systems* **2**(1), 1 – 9 – 9 (2016).

[27] Zimmerman, N. T., Eldorado Riggs, A. J., Jeremy Kasdin, N., Carlotti, A., and Vanderbei, R. J., "Shaped pupil Lyot coronagraphs: high-contrast solutions for restricted focal planes," *Journal of Astronomical Telescopes, Instruments, and Systems* **2**, 011012 (Jan 2016).

[28] Llop-Sayson, J., Ruane, G., Mawet, D., Jovanovic, N., Calvin, B., Levraud, N., Roberson, M., Delorme, J.-R., Echeverri, D., Klimovich, N., and Xin, Y., "Demonstration of an electric field conjugation algorithm for improved starlight rejection through a single mode optical fiber," *Journal of Astronomical Telescopes, Instruments, and Systems* **5**(1), 1 – 11 – 11 (2019).

[29] Coker, C. T., Shaklan, S. B., Riggs, A. J. E., and Ruane, G., "Simulations of a High-Contrast Single-Mode Fiber Coronagraphic Multi-Object Spectrograph for Future Space Telescopes," *arXiv e-prints*, arXiv:1907.03921 (Jul 2019).